BL-16A2/2020G537

Magnetic reversal in In-doped Mn_4N epitaxial films measured via x-ray magnetic dichroism

Tomohiro YASUDA[1], Taro KOMORI[1], Kenta AMEMIYA[2], and Takashi SUEMASU[1,*]
[1] University of Tsukuba, 1-1-1 Tennohdai, Tsukuba, Ibaraki, 305-8573, Japan
[2] Photon Factory, Institute of Materials Structure Science,
High Energy Research Organization,
1-1 Oho, Tsukuba, 305-0801, Japan

1 Introduction

Ferromagnetic alloys that combine non-magnetic and magnetic elements are ubiquitous in magnetism and spintronics. An intuitive rule of thumb is that the magnetic elements tend to favor the ferromagnetic phase. This has been seen, for instance, in usual 3d alloys such as Co-based materials, including CoPt, CoPd, and CoY [1-5]. In the following, we show the opposite behavior in In-doped Mn_4N, $Mn_{4-x}In_xN$ (x = 0.27 and 0.41), wherein decreasing the concentration of Mn, i.e., the concentration of the magnetic element of the alloy, favors the ferromagnetism. This astonishing behavior is then discussed based on the results of X-ray absorption spectroscopy (XAS) and X-ray magnetic circular dichroism (XMCD) measurements.

Over the past few years, there has been renewed interest in ferrimagnets for spintronics applications [6-14]. This is because we can control the magnetic moments of sublattices by doping various elements to reach an angular momentum compensation and/or magnetic compensation (MC) point. The transition of magnetic states by impurity doping has been suggested. For example, the phase transition from antiferromagnetic Mn_2Sb to ferrimagnetic $Mn_{2-x}Cr_xSb$ has been proposed by *ab initio* calculation [15]. Under such circumstances, we have paid particular attention to the rare-earth free ferrimagnet Mn_4N [16]. The unit cell of Mn_4N is described as a face-centered cubic (fcc) Mn cube with one N atom at the body center, and is composed of two Mn sublattices, i.e., Mn(I) atoms at corner sites and Mn(II) atoms at face-centered sites, with their magnetizations aligned antiparallel to each other [17]. Differently from Mn_4N bulk, Mn_4N films possess a perpendicular magnetic anisotropy (PMA) corresponding to a large magnetic anisotropy constant of ~10^5 J m^{-1} [18-21]. The PMA has been considered to originate from the in-plane tensile stress [18,22]. They also possess a spontaneous magnetization as small as ~100 kA m^{-1} [17,19,23], and a relatively high spin polarization of electrical conductivity (P = 0.8) [24]. By doping a small amount of magnetic elements, such as Ni or Co, and substituting for part of the Mn(I) and/or Mn(II) atoms, the MC can be reached at room temperature (RT) [25-27], with a high thermal stability [28]. The resulting spin-transport properties are astonishing, as the classical spin-transfer torque in these systems leads to domain wall velocities comparable to what can be obtained using spin–orbit torques. We have demonstrated a current-induced domain wall motion of 3,000 m s^{-1} in $(Mn,Ni)_4N$ at RT around the MC [29], and in excess of 900 m s^{-1} in Mn_4N [24]. The low spontaneous magnetization and high sensitivity to spin torques also make them excellent candidates for RT skyrmions applications and for radio-frequency oscillators [30]. Thus far, there has been a lot of studies on Mn_4N-based compounds such as $(Mn,A)_4N$(A = Fe [20], Ag [31], Au [32], In [33], Sn [33], Gd [34], and Dy [35,36]) and Mn_3BN (B = Ni [37], Cu [38], Zn [39-41], Ga [42-45], In [46], and Sn [47]). However, there has been no report on the existence of a ferrimagnetic-to-ferromagnetic transition at RT just by doping a non-magnetic element.

2 Experiment

$Mn_{4-x}In_xN$ (x = 0.15, 0.27, and 0.41) layers were epitaxially grown at 450 °C on MgO(001) by molecular beam epitaxy using a radio-frequency nitrogen plasma and standard Knudsen cells for In and Mn solid sources, followed by approximately 2-nm-thick Pt capping layers by in situ sputtering to prevent the oxidation of sample surface. Prior to thin-film growth, MgO(001) substrates were ultrasonically cleaned with aceton, methanol, and water, followed by pre-heating at 600 °C for 30 min in the growth chamber. The base pressure of the chamber was 1.3 × 10^{-7} Pa, and it increased to 4.8 × 10^{-3} Pa during the growth. The growth rate of $Mn_{4-x}In_xN$ layers was approximately 1.0 nm/min. The layers' crystallinity was characterized using out-of-plane (θ-2θ) and in-plane (φ-$2\theta_\chi$) x-ray diffractions (SmartLab, Rigaku Inc.) with a Cu-Kα radiation source. X-ray reflectometry (XRR) was used to measure the film thicknesses. Reflection high-energy electron diffraction (RHEED) was also used. The atomic compositions of the grown layers were evaluated by Rutherford backscattering spectroscopy (RBS), using He^+ ions accelerated at 2.0 MeV. Anomalous Hall effect (AHE) measurements were performed at RT by a physical property measurement system (PPMS, Quantum Design). We measured XAS and XMCD spectra at BL-16A of KEK Photon Factory in Japan, wherein the twin APPLE-II type undulator was

adopted. For reference, Mn_4N epitaxial layers (20 nm) were used for XAS and XMCD measurements. Both circularly polarized X-rays and ±5 T magnetic fields were applied at the magic angle (54.7°) from the sample normal [48]. The incident soft X-rays energy was set to include the Mn L_2 and L_3 absorption edges. In total electron yield (TEY) mode, the XAS spectra were acquired. Sample preparation details are summarized in Table 1.

Table 1. Sample preparation details: In composition (x), layer thicknesses of $Mn_{4-x}In_xN$ (d_{MnInN}) and Pt (d_{Pt}) measured using XRR are specified.

x	d_{MnInN} (nm)	d_{Pt} (nm)
0	25.1	1.7
0.15	28.7	2.5
0.27	26.1	1.7
0.41	23.9	2.5

3 Results and Discussion

Figures 1(a)-1(d) show the XAS and XMCD spectra at the Mn $L_{2,3}$ absorption edges measured on $Mn_{4-x}In_xN$ epitaxial layers (x = 0, 0.15, 0.27, and 0.41). There was not much difference in the XAS spectra of all the samples. The obtained XAS spectra are quite similar to those at the Mn $L_{2,3}$ absorption edges in $(Mn,Ni)_4N$ [25] and $(Mn,Co)_4N$ [26] epitaxial layers. A distinct shoulder is observed in the XAS spectra at a 2-eV higher energy than the main peaks of L_3 edges in all the films, as denoted by the arrows. Such shoulders have been reported for other anti-perovskite nitrides such as Fe_4N [49] and Co_4N [50]. According to first-principles calculation for Mn_4N [27] and Fe_4N [49], we ascribe the shoulder to the electric dipole transition from the Mn(Fe) 2p state to the hybrid state formed by the orbitals of the N 2p and Mn(Fe) 3d at II sites, suggesting that Mn(Fe) atoms at I sites exhibit more localized states than those at II sites. The XMCD spectra can therefore be understood as the addition of localized components plus itinerant components featured by peaks α and β, respectively, which have different signs for Mn_4N as shown in Fig. 1(a). Such features are reproduced well by first-principles calculation using the all-electron full-potential linearized augmented-plane-wave method and Fermi's golden rule with E1 transitions [27]. The opposite sign in peaks α and β means that Mn_4N is a ferrimagnet, wherein the magnetic moment of Mn(I) is aligned antiparallel to that of Mn(II) [27]. This difference arises from the difference in interatomic distance between N and Mn(I) atoms, and N and Mn(II) atoms. Based on the above discussion, we discuss the XMCD spectra of In-doped Mn_4N films. Differently from the XAS spectra, the XMCD spectra were rather complex and were significantly dependent on x. At x = 0.15, as shown in Fig. 1(b), the peak intensities of α and β decrease compared with those in Mn_4N, in Fig. 1(a), suggesting that the In atoms replace part of the Mn atoms at both I and II sites. When x is increased further to 0.27, the sign of peak β reverses, as shown in Fig. 1(c), while the sign of peak α remains unchanged, meaning that the magnetic moment of the Mn(II) atoms reverses and now aligns parallel to that of Mn(I). This relationship between α and β peaks holds at x = 0.41, as shown in Fig. 1(d). These results show that a ferrimagnetic-to-ferromagnetic transition appears when the In composition is increased up to x = 0.27 and 0.41.

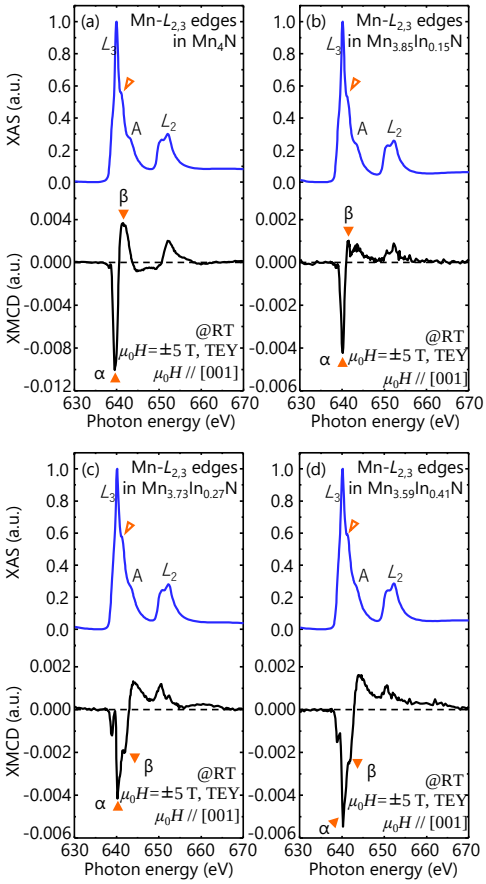

Fig. 1: XAS and XMCD spectra in (a) Mn_4N, (b) $Mn_{3.85}In_{0.15}N$, (c) $Mn_{3.73}In_{0.27}N$, and (d) $Mn_{3.59}In_{0.41}N$ epitaxial layers at the Mn $L_{2,3}$ absorption edges. The sharp peak (α) and broad peak (β) originate mainly from Mn(I) and Mn(II), respectively. The opposite signs of these XMCD signals show that the magnetic moment of Mn(I) aligns antiparallel to that of Mn(II). The sign reversal of peak (β) between (b) and (c) suggests the reversal of the magnetic moments of Mn(II).

Acknowledgement

This work is support in part by the Japan Society for the Promotion of Science (JSPS) KAKANHI (Grants Nos. JP19K04499, JP19K21954, and JP19KK0104). T.K. acknowledges additional support from the JSPS Fellows (No. 21J10330). The XAS and XMCD measurements were performed at BL-16A of KEK-PF (Proposal No. 2020G537). The authors thank Associate Professor T. Koyano of the Cryogenic Division, University of Tsukuba, for his help in the AHE measurements. RBS measurement was conducted at the Nanotechnology Platform of Hiroshima University.

References

[1] P. Mohn and E. P. Wohlfarth, J. Phys. F: Met. Phys. **17**, 2421 (1987).
[2] J. M. Sanchez *et al*., J. Phys. : Condens. Matter. **1**, 491 (1989).
[3] A. Kashyap *et al*., Phys. Rev. B **60**, 2262 (1999).
[4] T. Mehaddene *et al*., Phys. Rev. B **69**, 024304 (2004).
[5] L. Rohman *et al*., J. Phys.: Conf. Ser. **1170**, 012018 (2019).
[6] T. Okuno *et al*., Appl. Phys. Express **9**, 073001 (2016).
[7] J. Yu *et al*., Sci. Rep. **6**, 32629 (2016).
[8] S.-H. Oh *et al*., Phys. Rev. B **96**, 100407(R) (2017).
[9] K.-J. Kim *et al*., Nat. Mater. **16**, 1187 (2017).
[10] L. Caretta *et al*., Nat. Nanotechnol. **13**, 1154 (2018).
[11] Y. Hirata *et al*., Phys. Rev. B **97**, 220403(R) (2018).
[12] S. A. Siddiqui *et al*., Phys. Rev. Lett. **121**, 057701 (2018).
[13] R. Bläsing *et al*., Nat. Commun. **9**, 4984 (2018).
[14] K. Cai *et al*., Nat. Electron. **3**, 37 (2020).
[15] J. H. Wijngaard *et al*., Phys. Rev. B **45**, 5395 (1992).
[16] T. Suemasu *et al*., J. Phys. Soc. Jpn. **90**, 081010 (2021).
[17] W. J. Takei *et al*., Phys. Rev. **125**, 1893 (1962).
[18] Y. Yasutomi *et al*., J. Appl. Phys. **115**, 17A935 (2014).
[19] K. Kabara and M. Tsunoda, J. Appl. Phys. **117**, 17B512 (2015).
[20] A. Anzai *et al*., J. Cryst. Growth **489**, 20 (2018).
[21] T. Komori *et al*., J. Cryst. Growth **507**, 163 (2019).
[22] T. Hirose *et al*., AIP Adv. **10**, 025117 (2020).
[23] T. Gushi *et al*., Jpn. J. Appl. Phys. **57**, 120310 (2018).
[24] T. Gushi *et al*., Nano Lett. **19**, 8716 (2019).
[25] T. Komori *et al*., J. Appl. Phys. **127**, 043903 (2020).
[26] H. Mitarai *et al*., Phys. Rev. Mater. **4**, 094401 (2020).
[27] K. Ito *et al*., Phys. Rev. B **101**, 104401 (2020).
[28] W. Zhou *et al*., AIP Adv. **11**, 015334 (2021).
[29] S. Ghosh *et al*., Nano Lett. **21**, 2580 (2021).
[30] B. Dieny *et al*., Nat. Electron. **3**, 446 (2020).
[31] S. Deng *et al*., Solid State Commun. **222**, 37(2015).
[32] D. Li *et al*., Mater. Res. Bull. **122**, 110646(2020).
[33] M. Mekata, J. Phys. Soc. Jpn. **17**, 796 (1962).
[34] H. Li *et al*., J. Appl. Phys. **124**, 093903 (2018).
[35] M. Meng *et al*., J. Appl. Phys. **118**, 053911 (2015).
[36] M. Meng *et al*., Appl. Phys. Lett. **109**, 082405 (2016).
[37] M. Wu *et al*., J. Appl. Phys. **114**, 123902 (2013).
[38] K. Takenaka *et al*., J. Appl. Phys. **110**, 023909 (2011).
[39] B. Y. Qu, and B. C. Pan, J. Appl. Phys. **108**, 113920 (2010).
[40] T. Hamada, and K. Takenaka, J. Appl. Phys. **111**, 07A904 (2012).
[41] Y. Sun *et al*., Inorg. Chem. **51**, 7232(2012).
[42] T. Hajiri *et al*., Appl. Phys. Lett. **115**, 052403 (2019).
[43] D. Matsunami *et al*., Nat. Mater. **14**, 73(2015).
[44] K. Takenaka *et al*., J. Phys. Soc. Jpn. **90**, 044601 (2021).
[45] K. Shi *et al*., Adv. Mater. **28**, 3761 (2016).
[46] Y. S. Sun *et al*., J. Phys.: Conf. Ser. **400**, 032094 (2012).
[47] Y. You *et al*., Appl. Phys. Lett. **117**, 222404 (2020).
[48] J. Stöhr and H. König, Phys. Rev. Lett. **75**, 3748 (1995).
[49] K. Ito *et al*., J. Appl. Phys. **117**, 193906 (2015).
[50] K. Ito *et al*., J. Appl. Phys. **115**, 11C712 (2014).
[51] H. Ohno *et al*., Appl. Phys. Lett. **69**, 363 (1996).
[52] G. Kresse and J. Hafner, Phys. Rev. B **47**, 558 (1993).
[53] G. Kresse and D. Joubert, Phys. Rev. B **59**, 1758 (1999).
[54] J. P. Perdew *et al*., Phys. Rev. Lett. **77**, 3865 (1996).
[55] N. T. Nam and L. Ranno, J. Magn. Magn. Mater. **322**, 1428 (2010).
[56] S. J. Greaves *et al*., J. Magn. Magn. Mater. **235**, 418 (2001).

* suemsu.takashi.gu@u.tsukuba.ac.jp